



## Article

# Comprehensive Analysis and Validation of the Atmospheric Weighted Mean Temperature Models in China

Yongjie Ma <sup>1</sup>, Qingzhi Zhao <sup>1</sup>, Kan Wu <sup>2,\*</sup>, Wanqiang Yao <sup>1</sup>, Yang Liu <sup>3</sup>, Zufeng Li <sup>4</sup> and Yun Shi <sup>1</sup>

<sup>1</sup> College of Geomatics, Xi'an University of Science and Technology, Xi'an 710054, China; 20210226098@stu.xust.edu.cn (Y.M.); zhaoqingzhia@xust.edu.cn (Q.Z.); sxywq@xust.edu.cn (W.Y.); shiyun0908@xust.edu.cn (Y.S.)

<sup>2</sup> Key Laboratory of Aerospace Medicine of Ministry of Education, School of Aerospace Medicine, Air Force Medical University, Xi'an 710032, China

<sup>3</sup> School of Geodesy and Geomatics, Wuhan University, Wuhan 430079, China; liuyangre@whu.edu.cn

<sup>4</sup> Powerchina Northwest Engineering Corporation Limited, Xi'an 710000, China; lizufeng@xust.edu.cn

\* Correspondence: wukanhyx@fmmu.edu.cn; Tel.: +86-18821781969

**Abstract:** Atmospheric weighted mean temperature ( $T_m$ ) is a key parameter used by the Global Navigation Satellite System (GNSS) for calculating precipitable water vapor (PWV). Some empirical  $T_m$  models using meteorological or non-meteorological parameters have been proposed to calculate PWV, but their accuracy and reliability cannot be guaranteed in some regions. To validate and determine the optimal  $T_m$  model for PWV retrieval in China, this paper analyzes and evaluates some typical  $T_m$  models, namely, the Linear, Global Pressure and Temperature 3 (GPT3), the  $T_m$  model for China ( $CT_m$ ), the Global Weighted Mean Temperature-H ( $GT_m$ -H) and the Global Tropospheric (GTrop) models. The  $T_m$  values of these models are first obtained at corresponding radiosonde (RS) stations in China over the period of 2011 to 2020. The corresponding  $T_m$  values of 87 RS stations in China are also calculated using the layered meteorological data and regarded as the reference. Comparison results show that the accuracy of these five  $T_m$  models in China has an obvious geographical distribution and decreases along with increasing altitude and latitude, respectively. The average root mean square (RMS) and Bias for the Linear, GPT3,  $CT_m$ ,  $GT_m$ -H and GTrop models are 4.2/3.7/3.4/3.6/3.3 K and 0.7/−1.0/0.7/−0.1/0.3 K, respectively. Among these models, Linear and GPT3 models have lower accuracy in high-altitude regions, whereas  $CT_m$ ,  $GT_m$ -H and GTrop models show better accuracy and stability throughout the whole China. These models generally have higher accuracy in regions with low latitude and lower accuracy in regions with middle and high latitudes. In addition, Linear and GPT3 models have poor accuracy in general, whereas  $GT_m$ -H and  $CT_m$  models are obviously less accurate and stable than GTrop model in regions with high latitude. These models show different accuracies across the four geographical regions of China, with GTrop model demonstrating the relatively better accuracy and stability. Therefore, the GTrop model is recommended to obtain  $T_m$  for calculating PWV in China.

**Keywords:** atmospheric weighted mean temperature; Global Navigation Satellite System; empirical  $T_m$  model; accuracy analysis and evaluation



**Citation:** Ma, Y.; Zhao, Q.; Wu, K.; Yao, W.; Liu, Y.; Li, Z.; Shi, Y. Comprehensive Analysis and Validation of the Atmospheric Weighted Mean Temperature Models in China. *Remote Sens.* **2022**, *14*, 3435. <https://doi.org/10.3390/rs14143435>

Academic Editors: Xiaoming Wang, Kefei Zhang, Suelynn Choy, Karina Wilgan and Haobo Li

Received: 21 May 2022

Accepted: 14 July 2022

Published: 17 July 2022

**Publisher's Note:** MDPI stays neutral with regard to jurisdictional claims in published maps and institutional affiliations.



**Copyright:** © 2022 by the authors. Licensee MDPI, Basel, Switzerland. This article is an open access article distributed under the terms and conditions of the Creative Commons Attribution (CC BY) license (<https://creativecommons.org/licenses/by/4.0/>).

## 1. Introduction

Atmospheric water vapor is an important greenhouse gas in the atmosphere that plays an important role in climate change and weather forecasting [1]. Therefore, monitoring water vapor with high precision is critical for related studies. The Global Navigation Satellite System (GNSS) receiver can provide continuous and accurate values of precipitable water vapor (PWV) in the zenithal direction over a GNSS station, consequently the high temporal and spatial resolution PWV can be obtained when a dense network of GNSS stations is available [2]. Atmospheric weighted mean temperature ( $T_m$ ) is a key parameter in retrieving precipitable water vapor (PWV) using GNSS technology and its accuracy

will directly affect the PWV retrieval [3,4]. Although the radiosonde (RS) measurements have uncertainties, especially in terms of humidity, they are measured in land-atmosphere coupling (LoCo) in the atmosphere, and therefore can be considered the best information to use as a reference in the evaluation of  $T_m$  model [5]. Therefore, some regional or global  $T_m$  models using meteorological or non-meteorological parameters have been developed and used for PWV retrieval [6,7], and the  $T_m$  obtained by these models can more easily meet the requirements of PWV retrieval when compared with traditional techniques. In addition, some  $T_m$  models that are consistent with the research regions have also been established [8–10].

$T_m$  models are generally divided into two types depending on whether meteorological parameters are considered in calculating  $T_m$ . The first type of model considers the input of the measured meteorological parameters. Bevis model is the most representative model [11], which builds a linear regression equation between  $T_m$  and surface temperature ( $T_s$ ). The Bevis model was first established for calculating  $T_m$  in mid-latitude regions using the data of 8718 RS stations in the United States over the period of 1990–1991 and could calculate  $T_m$  using  $T_s$  according to the linear relationship. This model is relatively simple to use and can obtain higher accuracy in mid-latitude regions. In practical applications, this model shows no evident advantage compared with empirical models and the accuracy of  $T_m$  in other regions cannot be easily guaranteed [12]. The second type of model includes empirical  $T_m$  models without the input of measured meteorological parameters, which are obtained by applying the fitting method on global or local regions and require only the parameters of station location and time information. Therefore, these models can conveniently obtain the  $T_m$  [13,14]. In recent years, some empirical models, such as the series models of Global Pressure and Temperature (GPT) [15–17], Global Weighted Mean Temperature ( $GT_m$ ) [18,19], Global Tropospheric Model (GTrop) [20] and the  $T_m$  model for China ( $CT_m$ ) [21], have been proposed. Among the GPT models, the Global Pressure and Temperature 3 (GPT3) model not only has the highest accuracy [22] but also used an improved mapping function for coefficients to avoid the effect of low elevation angles [23]. However, this model ignores the vertical correction of  $T_m$ , hence making the error with altitude change more obvious [24,25]. Yao et al. [26] investigated the distribution characteristics of  $T_m$  in the vertical direction using the European Centre for Medium-Range Weather Forecasts (ECMWF) reanalysis data and further proposed a Global Weighted Mean Temperature-H ( $GT_m$ -H), which can significantly improve the reduction effect of  $T_m$  in the vertical direction. The  $T_m$  profile calculated by this model is also closer to the reference value compared with those calculated by other models. The GTrop model is established based on the ECMWF reanalysis data over the period of 1979 to 2017, which can provide  $T_m$  with a global spatial resolution of  $1^\circ \times 1^\circ$  and the accuracy of this model is significantly improved especially in high-altitude regions [27]. The  $CT_m$  model is established using the  $T_m$  recorded by the Global Geodetic Observing System (GGOS) at 540 grid points over the period of 2007 to 2014 [28]. This model considers the large topographic fluctuations and lapse rate function of  $T_m$  in China and can provide high-precision and real-time  $T_m$  only by inputting time and station location information. In terms of the performances of these empirical  $T_m$  models, they do not require any input of meteorological parameters and considers the temporal and spatial variation characteristics of  $T_m$ , hence making this model very useful for those users who cannot obtain surface temperature and demand relatively high accuracy [29]. The  $CT_m$  model takes into account the vertical lapse rate change of  $T_m$  and shows a significant advantage in China, especially in the Qinghai-Tibet Plateau region [30]. The GPT3 model is significantly affected by latitude; specifically, its error increases along with latitude, whereas its stability gradually decreases from the equator to the poles [31]. The  $GT_m$ -H model describes the effect of a nonlinear change in temperature on the  $T_m$  profile and considers the nonlinear altitude reduction, which can significantly improve the reduction effect of  $T_m$  in the vertical direction; this model is also the most accurate among all  $GT_m$  series models [32]. The GTrop model was established using data covering up to 40 years and demonstrates linear trends and seasonal effects in  $T_m$  changes;

in addition, this model also takes lapse rate into account to improve its height correction performance [33].

Although the performance of two types of  $T_m$  models have been evaluated previously on the regional or global scale, their stability and applicability have never been investigated before in China. In order to evaluate the applicability of five typical  $T_m$  models in China, namely, the linear, GPT3,  $CT_m$ ,  $GT_m$ -H and GTrop models, are evaluated from the perspectives of different altitudes, different latitudes, and different geographical regions, and then the most suitable  $T_m$  model was determined. The corresponding  $T_m$  values at 87 RS stations over the period of 2011 to 2020 in China, which are considered as the reference in this paper, are also calculated using layered meteorological data.

## 2. Data and Methods

### 2.1. Data Description

RS data are derived from the RS dataset of the National Climatic Data Center, which is available from the Integrated Global Radiosonde Archive Version 2 (IGRA2) dataset. IGRA2 implemented several enhancements to accommodate characteristics that are not present in IGRA1 and to improve the quality of the final wind and humidity data. IGRA2 also includes more RS stations and longer recordings compared with IGRA1 [34]. This dataset covers almost 2700 global stations for both RS and pilot balloon observations dating from 1960 to present and can be downloaded for free online (<ftp://ftp.ncdc.noaa.gov/pub/data/igra/>, accessed on 1 July 2021) [35]. RS data can provide the vertical profiles of meteorological parameters, including temperature, geopotential, and water vapor pressure, usually two or four times a day [36]. In this paper, RS data with the temporal resolution of two times (UTC 00:00 and 12:00) daily are selected from 87 RS stations in China over the period between 2011 to 2020. Given that  $T_m$  is highly related to geographical location, this study divides China into four geographical divisions. Figure 1 presents the geographical distribution of the 87 selected RS stations and the four geographical divisions of China.

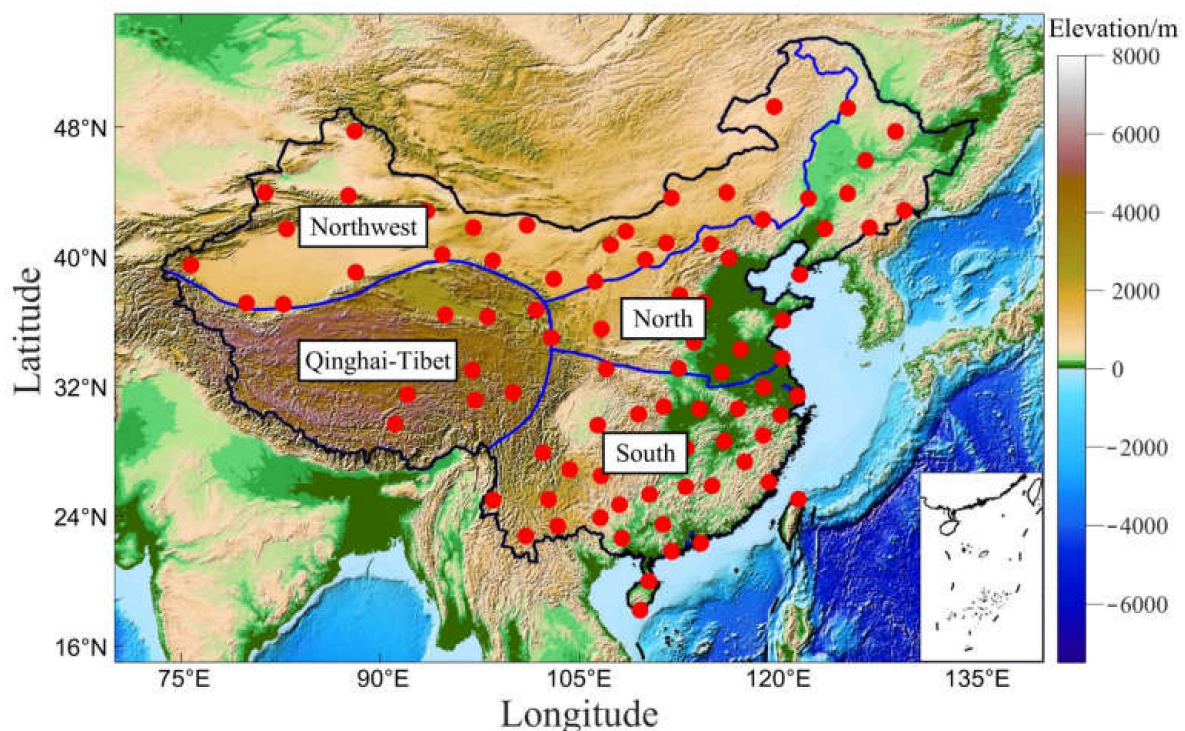


**Figure 1.** Geographical distribution of the 87 selected RS stations and the four geographical divisions of China.

## 2.2. Data Pre-Processing

Given the influence of external conditions, outliers in time series are inevitable when collecting data using meteorological sensors. As these outliers can adversely affect the further analysis, they should be removed at the data preprocessing period [37,38]. Interquartile range (IQR) is a commonly used method for outlier detection whose principle is to arrange a group of observation data from smallest to largest and then divide them into quartiles. The data in the 25th and 75th percentiles represent the lower and upper quartiles, respectively and the difference between them represents the IQR [39,40], which can be expressed as

$$\text{IQR} = Q_2 - Q_1 \quad (1)$$

where  $Q_1$  is the lower quartile,  $Q_2$  is the upper quartile;  $(Q_1, Q_2)$  covers the middlemost 50% of the data distribution. When the data fall in  $(Q_1 - 1.5 * \text{IQR}, Q_2 + 1.5 * \text{IQR})$ , the data dispersion is low and can be regarded as normal values; otherwise, the data are rejected as outliers.

## 2.3. $T_m$ Derived from RS Data

RS technology can obtain station-based meteorological parameters, such as temperature, pressure, potential height, and the relative humidity of different atmospheric layers. Given that these meteorological data are collected by meteorological sensors onboard an RS balloon, the  $T_m$  value calculated using these observed data has relatively high accuracy; Although RS has high accuracy in temperature profiles and uncertainty in humidity profiles, there is currently no better data source than RS for obtaining  $T_m$ , so RS can be considered as a reference for obtaining relatively better accuracy  $T_m$  [41]. RS provides meteorological data profiles in the form of layers and  $T_m$  is calculated as follows, according to the profile data of various meteorological parameters [42]:

$$T_m = \frac{\sum_{i=1}^n \frac{(z_2 - z_1)e_i}{T_i}}{\sum_{i=1}^n \frac{(z_2 - z_1)e_i}{T_i^2}} \quad (2)$$

where  $z_1$  and  $z_2$  are the altitude values of the upper and lower observation layers,  $e$  and  $T$  are the water vapor pressure and temperature over the observation layers, respectively. Although the  $T_m$  calculated by RS has relatively good accuracy and can be used as a reference to evaluate the accuracy of the  $T_m$  model, there is uncertainty in the calculation of  $T_m$  due to the uncertainty in the humidity measurement and this approach has low spatial and temporal resolutions [43,44].

## 2.4. $T_m$ Derived from Empirical Models

Five typical  $T_m$  models are selected in this paper, namely, the Linear, GPT3,  $CT_m$ ,  $GT_m$ -H and GTrop models, to evaluate their accuracy in China. Table 1 presents detailed information about these models, including their input parameters, application area, data used for modeling and selected data period.

### 1. Linear model

The Linear  $T_m$  model is established based on the linear regression equation of  $T_m$  and  $T_s$ . This model obtains  $T_m$  by simply inputting  $T_s$  at RS stations. In this paper, the linear relationship between  $T_m$  and  $T_s$  is established as follows using the RS data collected from 87 stations over the period of 2011 to 2020 in China:

$$T_m = 77.18 + 0.69T_s \quad (3)$$

where  $T_s$  is the surface temperature.

**Table 1.** Input parameters and application areas of the five selected  $T_m$  models.

Models	Input Parameters	Applicable Area	Data	Period
Linear	$T_s$	China	RS	2011–2020
GPT3	lat., lon., altitude, time	Global	ECMWF, VLBI	1999–2014
$CT_m$	lat., lon., altitude, time	China	GGOS	2007–2014
$GT_m$ -H	lat., lon., altitude, time	Global	ECMWF	2013–2015
GTrop	lat., lon., altitude, time	Global	ECMWF	1979–2017

## 2. GPT3 model

GPT3 is a commonly used global pressure and temperature empirical model that provides various parameters, such as pressure, water vapor pressure,  $T_m$ , temperature lapse rate, mapping function and gradient. Given its simple calculation and relatively high accuracy on global scale, GPT3 has been widely used in the geodetic and meteorological fields [45,46]. This model calculates  $T_m$  as

$$T_m = A_0 + A_1 \cos\left(\frac{\text{DOY}}{365.25} 2\pi\right) + B_1 \sin\left(\frac{\text{DOY}}{365.25} 2\pi\right) + A_2 \cos\left(\frac{\text{DOY}}{365.25} 4\pi\right) + B_2 \sin\left(\frac{\text{DOY}}{365.25} 4\pi\right) \quad (4)$$

where DOY is day of year,  $A_0$  is the mean value of  $T_m$ ,  $A_1$  and  $B_1$  are the coefficients of annual amplitude and  $A_2$  and  $B_2$  are the coefficients of semi-annual amplitude. In the  $T_m$  calculation of the GPT3 model, the coefficients and their amplitudes could be saved as a grid, from which the user then could spatially interpolate the desired position.

## 3. $CT_m$ model

The  $CT_m$  model is a grid empirical model that considers the annual and semi-annual periodic signals of  $T_m$  and the relationship between  $T_m$  and altitude. This model initially calculates the  $T_m$  value at the altitude of the grid point and then normalizes the  $T_m$  of the four grid points around an RS station to the altitude of this station. In this model,  $T_m$  can be calculated by inputting the longitude, latitude, altitude, and time of a specific RS station. The  $T_m$  model expression at grid point altitude is the same as that in Equation (4) and the  $T_m$  at the four-grid point altitude around the station are unified to station altitude, which can be expressed as

$$T_m^U = T_m^G - g \times (H_U - H_G) \quad (5)$$

where  $T_m^U$  denotes the  $T_m$  at the station altitude,  $T_m^G$  denotes the  $T_m$  at the grid point altitude,  $H_U$  and  $H_G$  denote the altitude at the station and grid point, respectively and  $g$  is the vertical lapse rate of  $T_m$ . After that, bilinear interpolation is carried out for the  $T_m^U$  of the four grid points with a unified altitude and the  $T_m$  at the RS station as calculated by the  $CT_m$  model is finally obtained.

## 4. $GT_m$ -H model

The  $GT_m$ -H model considers the nonlinear vertical reduction of  $T_m$  in high latitudes and describes the nonlinear variation of temperature on the  $T_m$  profile, which comprises two components, namely, the  $T_m$  at the mean sea level and the corrected value of  $T_m$  in the altitude direction. This model can be expressed as

$$T_m = T_m^{\text{MSL}} + T_m^h \quad (6)$$

$$T_m^h = \alpha_1 h + \alpha_2 \cos\left(\frac{2\pi h}{20}\right) + \alpha_3 \sin\left(\frac{2\pi h}{20}\right) \quad (7)$$

where  $T_m^{\text{MSL}}$  is the  $T_m$  at the mean sea level (K) that is calculated the same way as Equation (4),  $T_m^h$  is the  $T_m$  altitude correction value (K),  $h$  is the altitude (km),  $\alpha$  is the fitting parameter,  $\alpha_1$  represents the linear part of  $T_m^h$ ,  $\alpha_2$  and  $\alpha_3$  represent the nonlinear part of  $T_m^h$ .

## 5. GTrop model

The GTrop model considers the seasonal variations of  $T_m$  and uses the ERA-Interim reanalysis data over the period of 1979 to 2017 for the model construction, which provides

the  $T_m$  for a global  $1^\circ \times 1^\circ$  grid network [47]. This model calculates the  $T_m$  for each grid point as

$$T_m = [A_1 + A_2(Y - 1980) + A_3 \cos(\frac{DOY}{365.25} 2\pi) + A_4 \sin(\frac{DOY}{365.25} 2\pi) + A_5 \cos(\frac{DOY}{365.25} 4\pi) + A_6 \sin(\frac{DOY}{365.25} 4\pi)] - [A_7 + A_8(Y - 1980) + A_9 \cos(\frac{DOY}{365.25} 2\pi) + A_{10} \sin(\frac{DOY}{365.25} 2\pi) + A_{11} \cos(\frac{DOY}{365.25} 4\pi) + A_{12} \sin(\frac{DOY}{365.25} 4\pi)](h - h_0) \quad (8)$$

where  $Y$  denotes year,  $h_0$  is the altitude at the grid point (km),  $h$  is the altitude at the station (km) and  $A(i = 1 \sim 12)$  is the model coefficients of  $T_m$ . The  $T_m$  of a specific station is obtained via bilinear interpolation from the four nearby grid points of the station altitude.

### 2.5. Statistical Metrics for $T_m$ Model Evaluation

The  $T_m$  values derived from 87 RS stations are used as reference in evaluating the accuracy of the five typical models in China. The performance of these models is evaluated across different altitudes, latitudes, and geographical areas and over the entire area of China. Three evaluation indices are determined, namely, the root mean square (RMS), standard deviation (STD) and Bias. The standard deviation is used to measure the dispersion of a group of numbers, the RMS is used to measure the deviation between the observed value and the true value, and the Bias, is the average of the difference between the measured value and the true value. If the statistical distribution of the error is normal, then the probability of random error falling within  $\pm\sigma$  is 68%. The corresponding indices are computed as

$$RMS = \sqrt{\frac{1}{n} \sum_{i=1}^n v_i^2} \quad (9)$$

$$Bias = \frac{1}{n} \sum_{i=1}^n v_i \quad (10)$$

$$STD = \sqrt{\frac{1}{n} \sum_{i=1}^n (x_i - u)^2} \quad (11)$$

where  $v_i$  is the difference between the  $T_m$  derived from the empirical  $T_m$  models and RS data, and  $n$  is the total number of observed values. RMS is used to evaluate the overall accuracy of the empirical  $T_m$  models, whereas Bias is used to evaluate their average deviation.  $x_i$  is the  $T_m$  derived from the empirical  $T_m$  models and  $u$  is its average value.

## 3. Accuracy Analysis of $T_m$ Models

### 3.1. Accuracy Analysis at Different Altitudes

To verify the accuracy of the five typical  $T_m$  models at different altitudes, five RS stations with station names of 55299, 52836, 56691, 51644 and 58606 distributed in different altitudes are selected and the time series of  $T_m$  derived from the five models and the selected RS stations over the period of 2011 to 2020 are compared (Figure 2). As can be seen from Figure 2, the  $T_m$  value gradually decreases along with an increasing altitude. The  $T_m$  derived from the five models are generally consistent with that derived by the RS stations, but the corresponding values from the Linear model tend to be large at high altitudes. To further analyze the performance of these models in different altitudes, 87 RS stations in China are divided into five groups according to different altitudes, namely, [0, 500), [500, 1000), [1000, 1500), [1500, 2000) and [2000, 5000). Figure 3 presents the average RMS, STD, and Bias values for each group of RS stations over the period of 2011 to 2020. Comparison results show that the errors of the Linear model at different altitudes are all large and gradually increase along with altitude. A significant positive deviation and a large RMS are also observed in the altitude range, hence suggesting that the Linear model is not suitable for calculating  $T_m$  in high-altitude regions. The  $T_m$  derived from GPT3 model also shows a large RMS at altitudes exceeding 500 m. Meanwhile, the Bias results show that the  $T_m$  derived from the GPT3 model demonstrate obvious negative deviations at different altitudes. Among the five  $T_m$  models,  $CT_m$ ,  $GT_m$ -H and  $GTrop$  models have

the most stable accuracy, and their accuracy is significantly higher at altitudes exceeding 2000 m because they consider the effect of altitude on  $T_m$ . In addition, the  $T_m$  derived from Linear model shows the largest error among all models at different altitudes, followed by the GPT3 model. Meanwhile, the  $CT_m$ ,  $GT_m$ -H and GTrop models obtain relatively high accuracy, and their RMS tends to decrease along with increasing altitude and their Bias values are all less than 1 K at different altitudes. In general, GTrop model has the smallest RMS at different altitudes, which indicates its high accuracy and stability. The Linear and GTrop models do not greatly differ in their RMS value, which is around 3.5 K. However, with an increasing altitude, the RMS of these models shows an opposite trend. In the [2000, 5000) group, the RMS derived from Linear model reaches 5.7 K, whereas that of the GTrop model reaches only 2.7 K. The same difference between the Linear and GTrop model can also be observed in their Bias values. In the [2000, 5000) group, the Bias value of the Linear model reaches 4.0 K, whereas that of the GTrop model falls within the range of (0, 1) K at different altitudes. Therefore, at different altitudes, the GTrop model shows a larger advantage than the traditional model, while in the [2000, 5000) group, the  $CT_m$  model has relatively better accuracy.

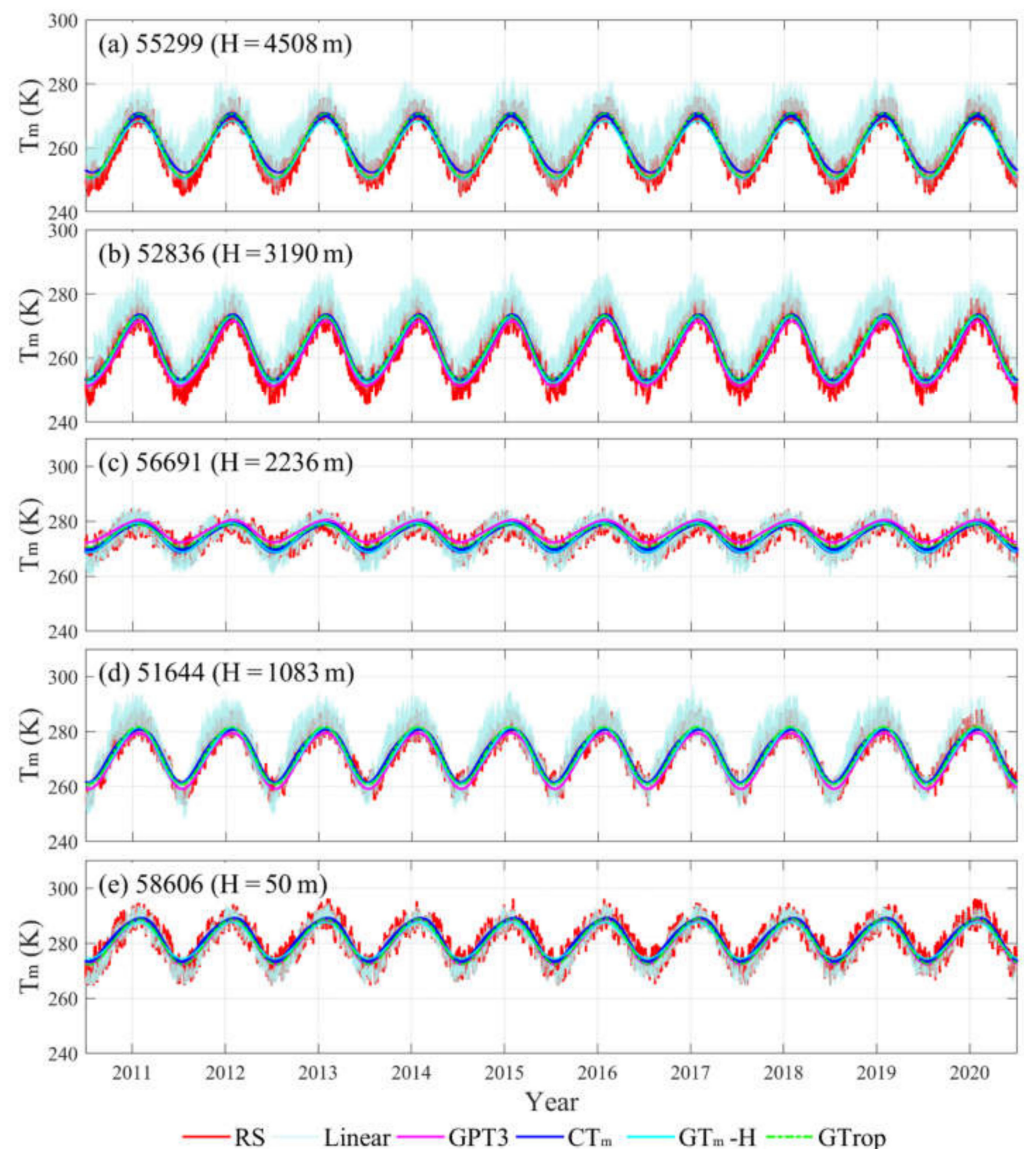


**Figure 2.** Time series comparison of the five  $T_m$  models and the RS-derived  $T_m$  at five stations distributed in different altitudes over the period of 2011 to 2020.

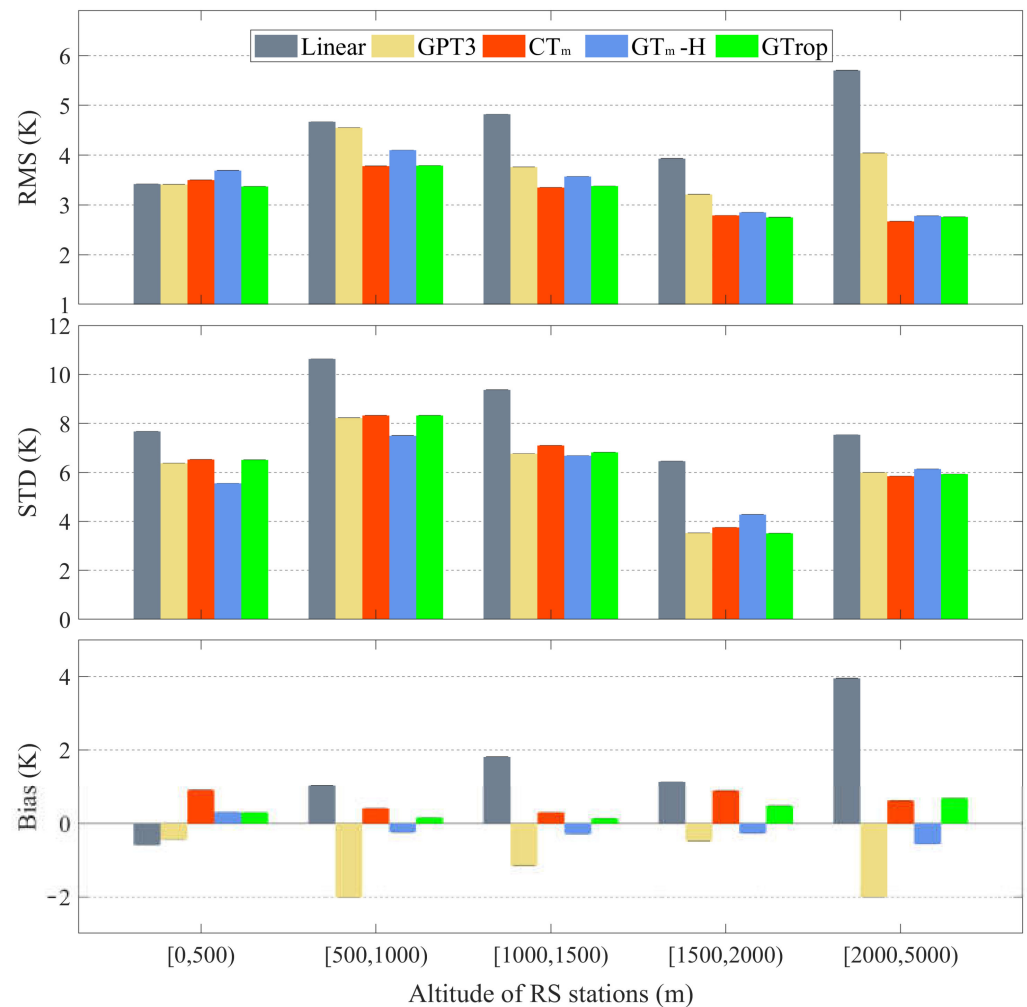


**Figure 3.** Average RMS and Bias of the five  $T_m$  models at different altitude ranges over the period of 2011 to 2020.

### 3.2. Accuracy Analysis at Different Latitudes

To further verify the accuracy of the five  $T_m$  models at different latitudes, 87 RS stations in China are divided into six groups, namely,  $[15^\circ, 25^\circ)$ ,  $[25^\circ, 30^\circ)$ ,  $[30^\circ, 35^\circ)$ ,  $[35^\circ, 40^\circ)$ ,  $[40^\circ, 45^\circ)$  and  $[45^\circ, 55^\circ)$ , according to their latitude. Figure 4 presents a time series comparison of the five typical  $T_m$  models at six RS stations with station names of 50774, 53068, 52866, 56146, 58633 and 59265 in different latitude groups. It can be observed that the  $T_m$  gradually decreases along with increasing latitude. In the low latitude region, the  $T_m$  derived by these models shows good consistency with that derived from the RS stations, but some differences are observed in the mid-latitude and high latitude regions, especially between the Linear and GPT3 model. Figure 5 presents the average RMS, STD and Bias statistics of these models at different latitudes over the period of 2011 to 2020. These five models obtain different accuracies across each latitude. In terms of RMS, the RMS of the five  $T_m$  models gradually increase along with latitude, the RMS of the Linear model is relatively large at different latitudes, the RMS of the CT<sub>m</sub> and GTrop models are small and do not increase much and the GT<sub>m</sub>-H model obtains a relatively large RMS at high latitudes  $[45^\circ, 55^\circ)$ . Meanwhile, the Bias comparison results show that the Linear model has a negative deviation in  $T_m$  at low latitudes and a positive deviation at mid- and high latitudes, the GPT3 model has negative deviations at different latitudes and the GT<sub>m</sub>-H and GTrop models have deviations of less than 1 K at different latitudes, especially at the mid- and high latitude regions where these models report smaller deviations compared with the

other models. In addition, the errors of the five  $T_m$  models gradually increase along with latitude. In general, both GTrop and  $CT_m$  models show relatively good performance at different latitudes. The RMS of  $CT_m$  is slightly smaller than that of GTrop model at middle latitudes [ $35^\circ$ ,  $40^\circ$ ), but GTrop model is better than  $CT_m$  model from the perspective of Bias index.

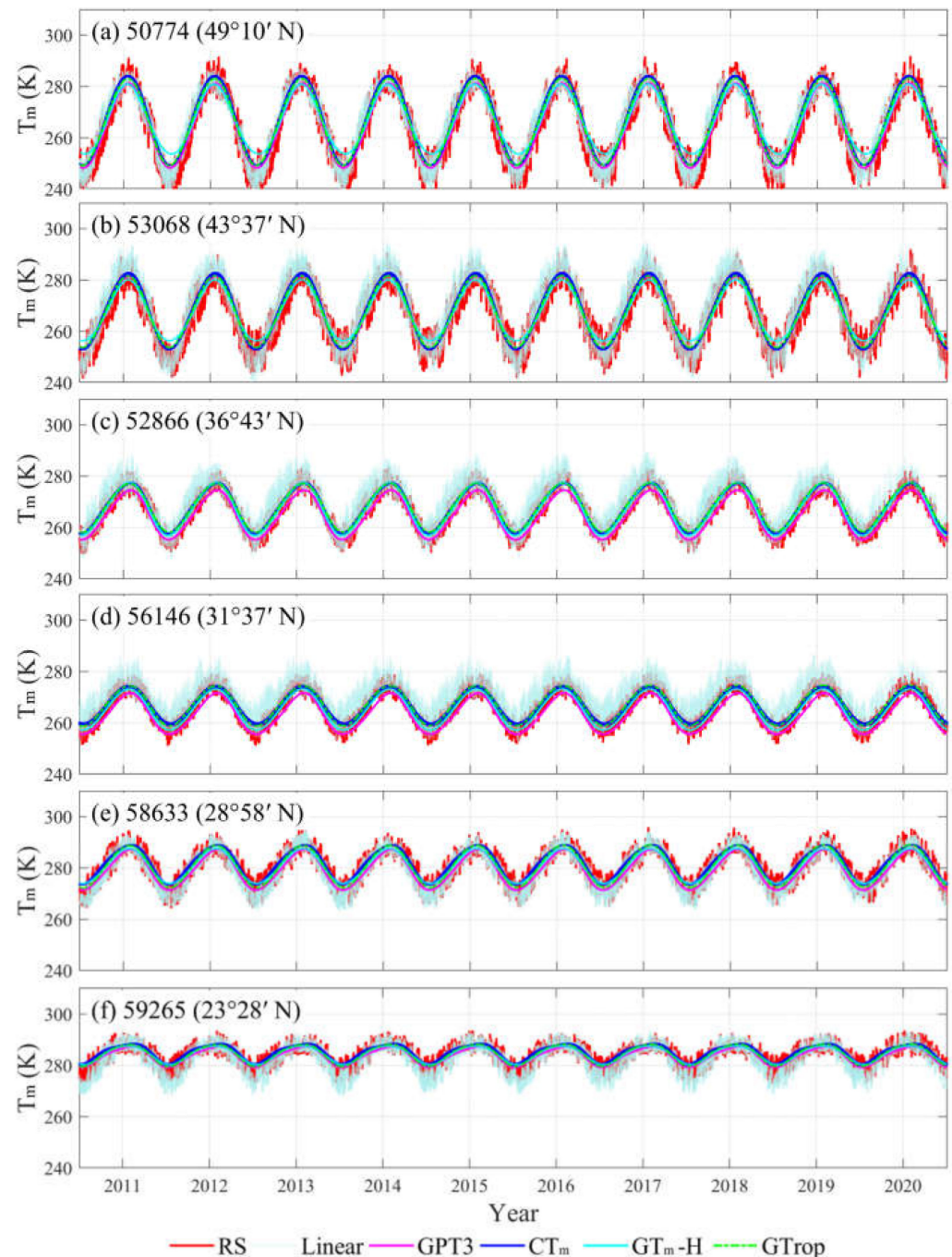


**Figure 4.** Time series comparison of the five  $T_m$  models and the RS-derived  $T_m$  at six stations distributed in different latitudes over the period of 2011 to 2020.

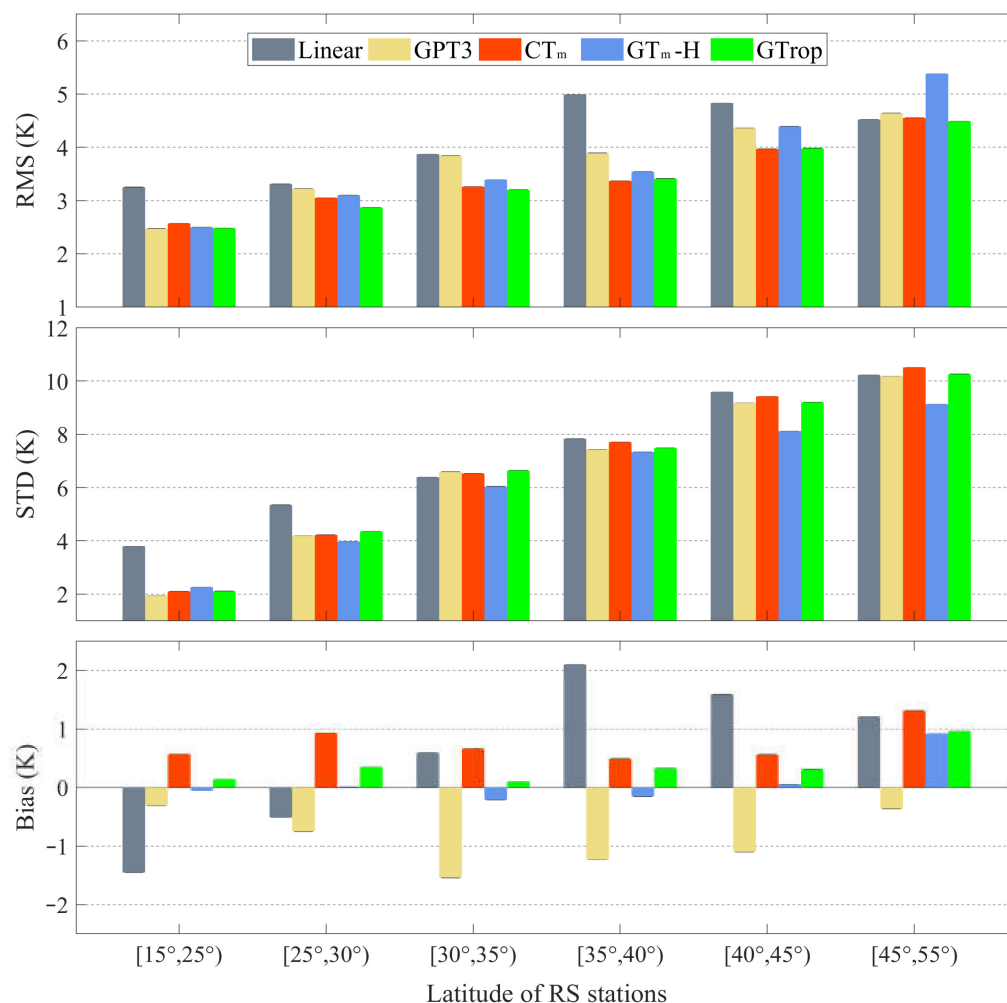


**Figure 5.** Average RMS and Bias of the five  $T_m$  models at different latitudes over the period of 2011 to 2020.

### 3.3. Accuracy Analysis at Different Geographical Regions in China

Given that  $T_m$  is affected by different locations and natural environments [48], China is divided into four geographical regions, namely, North (N), South (S), Northwest (NW) and Qinghai-Tibet (QT), to analyze the performance of the five typical  $T_m$  models. These regions have average altitudes of 0.3, 0.5, 1.1 and 3.3 km, respectively. A total of 20, 34, 24 and nine RS stations are distributed in regions of N, S, NW and QT, respectively. To evaluate the accuracy of the traditional and empirical models, Figure 6 shows the time series of  $T_m$  differences derived from the Linear and GTrop models at four RS stations with station names of 57178, 56964, 51644 and 52818 distributed in regions of N, S, NW, and QT over the period of 2011 to 2020. The  $T_m$  values derived by these empirical models exhibit some differences in four geographical regions of China. For instance, the  $T_m$  difference derived from the GTrop model is smaller than that of the Linear model, especially in the NW and QT regions but not in the N region. Therefore, the GTrop model should be used instead of the traditional Linear model in the QT region to obtain  $T_m$  with relatively better accuracy. Figure 7 shows the RMS and absolute Bias (ABias) of the five  $T_m$  models in four geographical regions. Here, the RMS and ABias presented in Figure 7 was calculated using all radiosonde stations located in each region. The accuracy of the  $T_m$  models shows different characteristics in each region. Specifically, the RMS values of these models in regions of N and NW are larger than those in region of S. Across all four geographical regions, the Linear model obtains the largest RMS value among all those models. This model also obtains the largest ABias value in regions of S and QT. Generally, the CT<sub>m</sub> and

GTrop models outperform the other empirical  $T_m$  models in the four geographical regions of China.

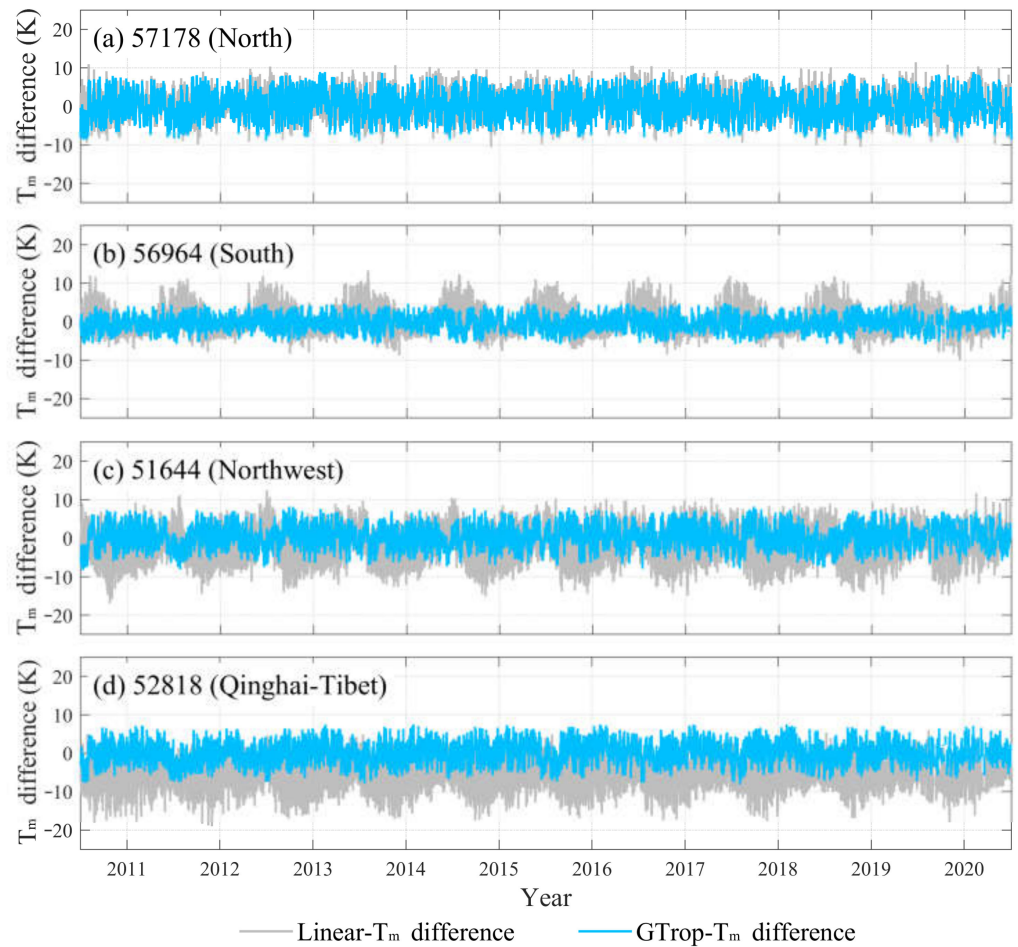


**Figure 6.** Comparison of  $T_m$  difference between the Linear/GTrop model and four RS stations distributed across the four geographical regions of China over the period of 2011 to 2020.

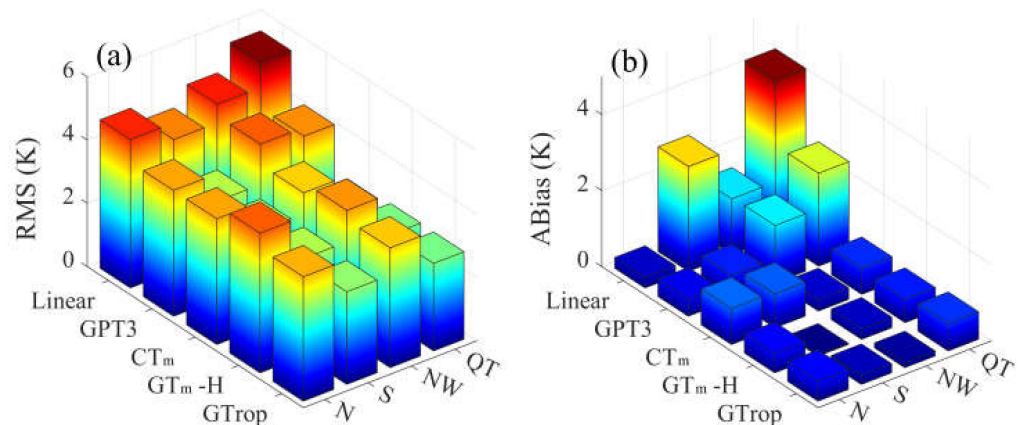


**Figure 7.** Average RMS and absolute Bias (ABias) of the five  $T_m$  models in the four geographical regions of China over the period of 2011 to 2020. (a) refers average RMS of the five  $T_m$  models in the four geographical regions of China over the period of 2011 to 2020 and (b) refers absolute Bias (ABias) of the five  $T_m$  models in the four geographical regions of China over the period of 2011 to 2020.

### 3.4. Overall Evaluation of $T_m$ Models in China

To validate the overall accuracy of the five typical  $T_m$  models in China, the corresponding  $T_m$  values at 87 RS stations in China over the period of 2011 to 2020 are compared with those derived by the empirical models. Figures 8 and 9 present RMS and Bias distributions of  $T_m$  difference between the RS and five typical  $T_m$  models, respectively. It can be observed that the  $CT_m$  and  $GTrop$  models show the best accuracy at high-altitude regions, whereas the Linear model present the lowest accuracy. The Bias of the Linear model is obviously large in NW region and smaller in S region of China, whereas that of GPT3 model is significantly smaller in NW. In addition, the ABias of the  $GT_m$ -H model is larger than that of the  $CT_m$  and  $GTrop$  models in QT region of China. In general, these empirical  $T_m$  models have better accuracy in low-latitude regions than in high-latitude regions.

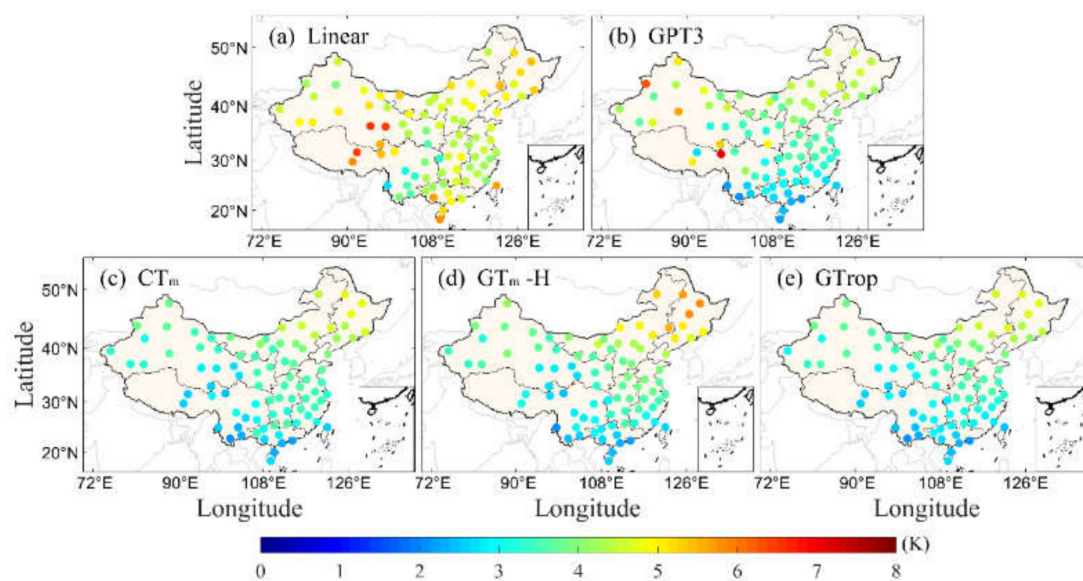


**Figure 8.** RMS distribution of the  $T_m$  difference between the five  $T_m$  models and the 87 RS stations in China over the period of 2011 to 2020.

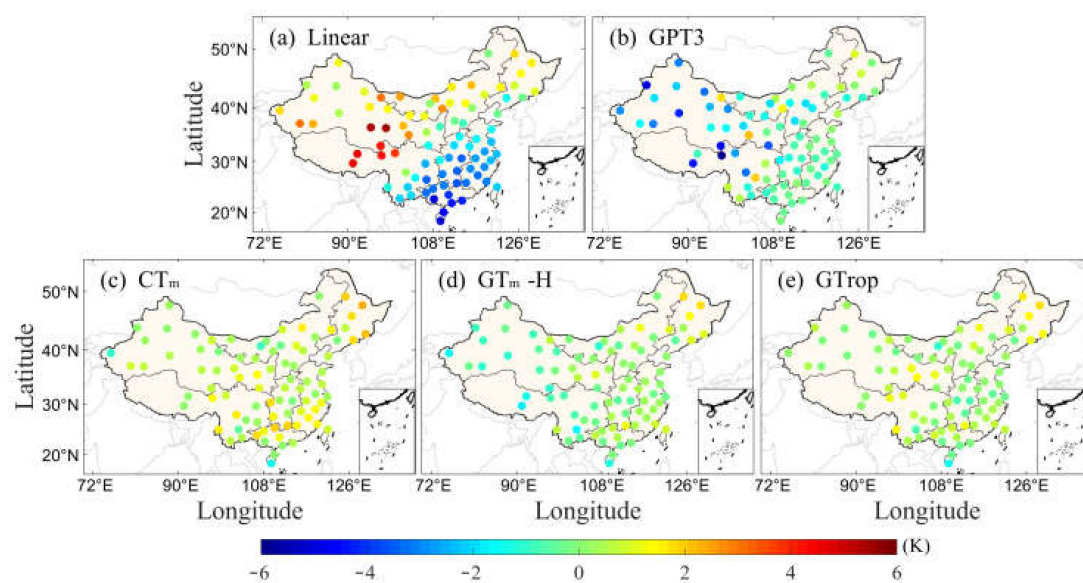


**Figure 9.** Bias distribution of the  $T_m$  difference between the five  $T_m$  models and the 87 RS stations in China over the period of 2011 to 2020.

Figures 10 and 11 present the percentages of RMS and Bias in different intervals as calculated by the five  $T_m$  models at 87 RS stations in China. It can be observed that the Linear model has a relatively large number of RS stations with large RMS and Bias values. Meanwhile, the GPT3 and  $G_{Tm}$ -H models have relatively few stations with RMS values exceeding 5 K, whereas the RMS value of  $CT_m$  and GTrop models is below 5 K. In addition, there are more stations with RMS value of  $T_m$  derived from GTrop model less than 3 K. The Bias values in the  $CT_m$ ,  $G_{Tm}$ -H and GTrop models are concentrated in  $(-1, 1)$  K, whereas that in the Linear and GPT3 models are below  $(-1, 1)$  K. Generally, the  $CT_m$ ,  $G_{Tm}$ -H and GTrop models have relatively better accuracy than that of the other models. Table 2 shows that the average RMS of the five models are 4.2, 3.7, 3.4, 3.6 and 3.3 K for the 87 stations, whereas their average Bias are 0.7,  $-1.0$ , 0.7,  $-0.1$  and 0.3 K, respectively. Generally, the GTrop model has the best accuracy among the five models followed by the  $CT_m$  model, whereas the Linear model demonstrates the worst accuracy.

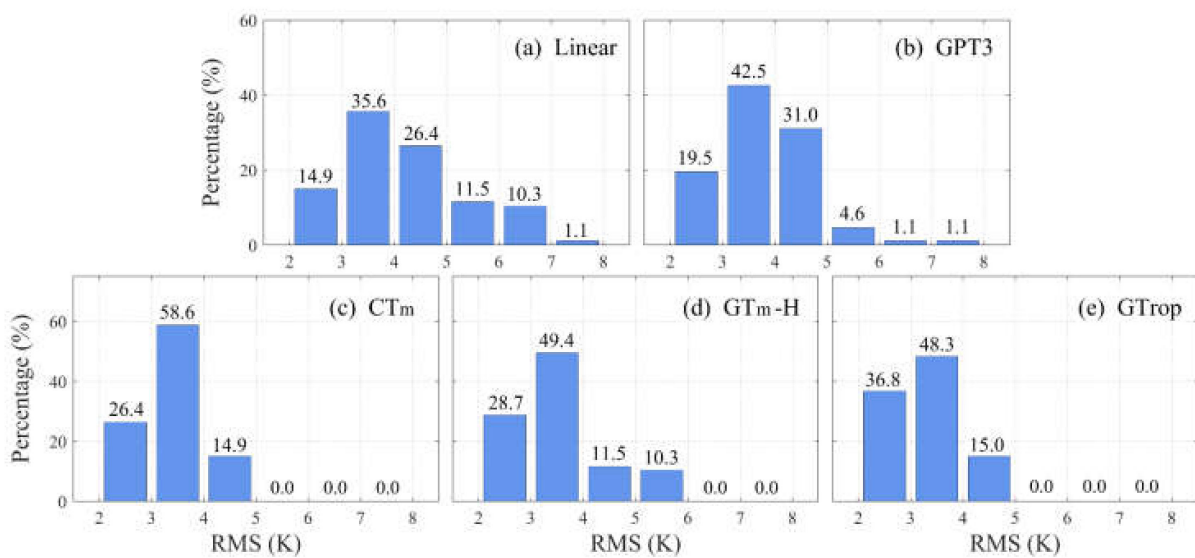


Figure 10. Percentage of RMS in different intervals calculated by the five  $T_m$  models at 87 RS stations over the period of 2011 to 2020.

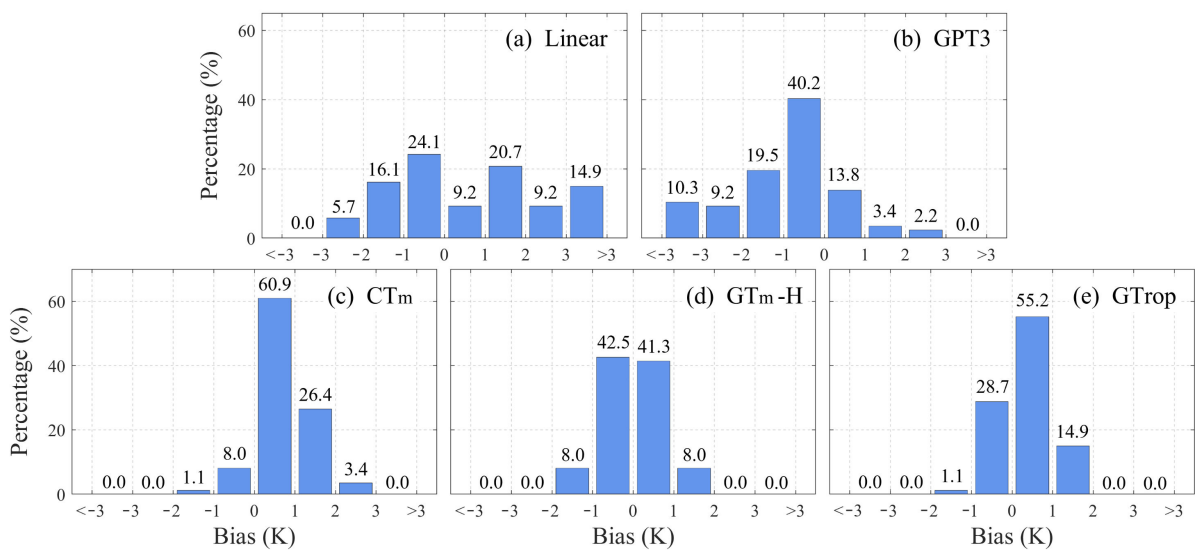


Figure 11. Percentage of Bias in different intervals calculated by the five  $T_m$  models at 87 RS stations over the period of 2011 to 2020.

**Table 2.** Average RMS and Bias of the five  $T_m$  models at 87 RS stations over the period of 2011 to 2020.

Model	RMS (K)			Bias (K)		
	Max.	Min.	Aver.	Max.	Min.	Aver.
Linear	7.1	2.1	4.2	5.9	−2.8	0.7
GPT3	7.1	2.1	3.7	2.1	−6.7	−1.0
$CT_m$	4.9	2.1	3.4	2.3	−1.4	0.7
$GT_m$ -H	5.8	2.0	3.6	1.9	−1.8	−0.1
GTrop	4.7	2.1	3.3	1.7	−1.4	0.3

#### 4. Conclusions

To determine the optimal  $T_m$  model to be used in China, the performances of five typical  $T_m$  models, namely, Linear, GPT3,  $CT_m$ ,  $GT_m$ -H and GTrop models, are compared and validated in this paper. Corresponding meteorological data of 87 RS stations over the period of 2011 to 2020 are selected to calculate  $T_m$  and as the reference. Although there is uncertainty, the RS measurements are based on LoCo technique and therefore can be considered the best for this evaluation. The performance and applicability of these  $T_m$  models are analyzed across different altitudes, latitudes, and geographical regions and for the entire China. Experimental results reveal that  $T_m$  shows obvious geographical characteristics in China and the accuracy of the selected  $T_m$  models generally decrease along with increasing altitude and latitude. The results obtained at different altitudes show that the Linear and GPT3 models are not suitable for calculating  $T_m$  in high-altitude regions, whereas the  $CT_m$ ,  $GT_m$ -H and GTrop models have relatively good accuracy due to their consideration of the effects of altitude. In addition, the GTrop model has relatively more advantages over the other models in terms of accuracy and stability. Meanwhile, the results obtained at different latitudes reveal that these empirical  $T_m$  models show higher accuracies in low-latitude areas, but such accuracy decreases in the mid and high latitudes. The Linear and GPT3 models have large errors, whereas the  $GT_m$ -H and  $CT_m$  models obtain high accuracy in high latitudes. Results obtained at different geographical regions also verified the relatively higher accuracy and stability of the GTrop model compared with the other  $T_m$  models. Therefore, the GTrop model is recommended for calculating  $T_m$  in China.

**Author Contributions:** Conceptualization, Y.M., Q.Z., K.W. and W.Y.; methodology, Y.M. and Q.Z.; software, Y.M. and K.W.; validation, K.W., Y.L., Z.L., W.Y. and Y.S.; writing—original draft preparation, Y.M. and Q.Z.; writing—review and editing, Q.Z., Y.S. and Y.L.; visualization, Q.Z., K.W., Y.S. and Y.L. All authors have read and agreed to the published version of the manuscript.

**Funding:** This research was supported by the Interdisciplinary joint research program of the department of aerospace medicine, Air Force Military Medical University (2021SZJC1004), key research and development plan of Shaanxi Province (2022SF-190) and Science and technology projects of Northwest Engineering Corporation Limited (XBY-KJ-2019-06 and XBY-KJ-2021-14).

**Data Availability Statement:** Not applicable.

**Acknowledgments:** Thanks to the National Climatic Data Center for providing the Radiosonde data. Michael Bevis, Daniel Landskron, Liangke Huang, Yibin Yao and Zhangyu Sun are also thanked for providing the corresponding  $T_m$  model.

**Conflicts of Interest:** The authors declare no conflict of interest.

#### References

1. Zhao, Q.; Liu, Y.; Yao, W.; Yao, Y. Hourly rainfall forecast model using supervised learning algorithm. *IEEE Trans. Geosci. Remote Sens.* **2021**, *60*, 4100509. [[CrossRef](#)]
2. Zhao, Q.; Liu, Y.; Ma, X.; Yao, W.; Yao, Y.; Li, L. An improved rainfall forecasting model based on GNSS observations. *IEEE Trans. Geosci. Remote Sens.* **2020**, *58*, 4891–4900. [[CrossRef](#)]
3. Huang, L.; Liu, L.; Chen, H.; Jiang, W. An improved atmospheric weighted mean temperature model and its impact on GNSS precipitable water vapor estimates for China. *GPS Solut.* **2019**, *23*, 51. [[CrossRef](#)]

4. Yao, Y.; Sun, Z.; Xu, C. Applicability of Bevis Formula at Different Height Levels and Global Weighted Mean Temperature Model Based on Near-earth Atmospheric Temperature. *J. Geod. Geoinf. Sci.* **2020**, *3*, 1–11.
5. Lee, S.-W.; Choi, B.I.; Woo, S.-B.; Kim, J.C.; Kim, Y.-G. Calibration of a radiosonde humidity sensor at low temperature and low pressure. *Metrologia* **2019**, *56*, 055008. [[CrossRef](#)]
6. Zhao, Q.; Ma, X.; Yao, W.; Liu, Y.; Yao, Y. A drought monitoring method based on precipitable water vapor and precipitation. *J. Clim.* **2020**, *33*, 10727–10741. [[CrossRef](#)]
7. Zhao, Q.; Du, Z.; Li, Z.; Yao, W.; Yao, Y. Two-Step Precipitable Water Vapor Fusion Method. *IEEE Trans. Geosci. Remote Sens.* **2021**, *60*, 5801510. [[CrossRef](#)]
8. Yao, Y.; Xu, C.; Zhang, B.; Cao, N. GTm-III: A new global empirical model for mapping zenith wet delays onto precipitable water vapour. *Geophys. J. Int.* **2014**, *197*, 202–212. [[CrossRef](#)]
9. Huang, L.; Jiang, W.; Liu, L.; Chen, H.; Ye, S. A new global grid model for the determination of atmospheric weighted mean temperature in GPS precipitable water vapor. *J. Geod.* **2019**, *93*, 159–176. [[CrossRef](#)]
10. Ding, M.; Hu, W. A further contribution to the seasonal variation of weighted mean temperature. *Adv. Space Res.* **2017**, *60*, 2414–2422. [[CrossRef](#)]
11. Bevis, M.; Businger, S.; Herring, T.A.; Rocken, C.; Anthes, R.A.; Ware, R.H. GPS meteorology: Remote sensing of atmospheric water vapor using the Global Positioning System. *J. Geophys. Res. Atmos.* **1992**, *97*, 15787–15801. [[CrossRef](#)]
12. Ding, M. A neural network model for predicting weighted mean temperature. *J. Geod.* **2018**, *92*, 1187–1198. [[CrossRef](#)]
13. Yang, F.; Guo, J.; Meng, X.; Shi, J.; Zhang, D.; Zhao, Y. An improved weighted mean temperature ( $T_m$ ) model based on GPT2w with  $T_m$  lapse rate. *GPS Solut.* **2020**, *24*, 46. [[CrossRef](#)]
14. Gao, W.; Gao, J.; Yang, L.; Wang, M.; Yao, W. A novel modeling strategy of weighted mean temperature in China using RNN and LSTM. *Remote Sens.* **2021**, *13*, 3004. [[CrossRef](#)]
15. Böhm, J.; Heinkelmann, R.; Schuh, H. Short note: A global model of pressure and temperature for geodetic applications. *J. Geod.* **2007**, *81*, 679–683. [[CrossRef](#)]
16. Lagler, K.; Schindelegger, M.; Böhm, J.; Krásná, H.; Nilsson, T. GPT2: Empirical slant delay model for radio space geodetic techniques. *Geophys. Res. Lett.* **2013**, *40*, 1069–1073. [[CrossRef](#)]
17. Böhm, J.; Möller, G.; Schindelegger, M.; Pain, G.; Weber, R. Development of an improved empirical model for slant delays in the troposphere (GPT2w). *GPS Solut.* **2015**, *19*, 433–441. [[CrossRef](#)]
18. Yao, Y.B.; Zhang, B.; Yue, S.Q.; Xu, C.Q.; Peng, E.F. Global empirical model for mapping zenith wet delays onto precipitable water. *J. Geod.* **2013**, *87*, 439–448. [[CrossRef](#)]
19. Yao, Y.; Zhang, B.; Xu, C.; Yan, F. Improved one/multi-parameter models that consider seasonal and geographic variations for estimating weighted mean temperature in ground-based GPS meteorology. *J. Geod.* **2014**, *88*, 273–282. [[CrossRef](#)]
20. Sun, Z.; Zhang, B.; Yao, Y. A global model for estimating tropospheric delay and weighted mean temperature developed with atmospheric reanalysis data from 1979 to 2017. *Remote Sens.* **2019**, *11*, 1893. [[CrossRef](#)]
21. Huang, L.; Peng, H.; Liu, L.; Li, C.; Kang, C.; Xie, S. An empirical atmospheric weighted mean temperature model considering the lapse rate function for China. *Acta Geod. Cartogr. Sin.* **2020**, *49*, 432–442.
22. Landskron, D.; Böhm, J. VMF3/GPT3: Refined discrete and empirical troposphere mapping functions. *J. Geod.* **2018**, *92*, 349–360. [[CrossRef](#)]
23. Nistor, S.; Suba, N.S.; Buda, A.S. The impact of tropospheric mapping function on PPP determination for one-month period. *Acta Geodyn. Geomater.* **2020**, *17*, 237–252. [[CrossRef](#)]
24. Mao, J.; Han, J.; Cui, T. Development and Assessment of Improved Global Pressure and Temperature Series Models. *IEEE Access* **2021**, *9*, 104429–104447. [[CrossRef](#)]
25. Li, T.; Wang, L.; Chen, R.; Fu, E.; Xu, W.; Jiang, P.; Liu, J.; Zhou, H.; Han, Y. Refining the empirical global pressure and temperature model with the ERA5 reanalysis and radiosonde data. *J. Geod.* **2021**, *95*, 31. [[CrossRef](#)]
26. Yao, Y.; Sun, Z.; Xu, C.; Xu, X. Global Weighted Mean Temperature Model Considering Nonlinear Vertical Reduction. *Geomat. Inf. Sci. Wuhan Univ.* **2019**, *44*, 106–111.
27. Zhu, M.; Hu, W.; Sun, W. Advanced grid model of weighted mean temperature based on feedforward neural network over China. *Earth Space Sci.* **2021**, *8*, e2020EA001458. [[CrossRef](#)]
28. Huang, L.; Zhu, G.; Liu, L.; Chen, H.; Jiang, W. A global grid model for the correction of the vertical zenith total delay based on a sliding window algorithm. *GPS Solut.* **2021**, *25*, 98. [[CrossRef](#)]
29. Mo, Z.X.; Huang, L.K.; Peng, H.; Liu, L.L.; Kang, C.L. Atmospheric Weighted Mean Temperature Model in Guilin. *Int. Arch. Photogramm. Remote Sens. Spat. Inf. Sci.* **2020**, *42*, 1155–1160. [[CrossRef](#)]
30. Huang, L.; Mo, Z.; Liu, L.; Xie, S. An empirical model for the vertical correction of precipitable water vapor considering the time-varying lapse rate for Mainland China. *Acta Geod. Cartogr. Sin.* **2021**, *50*, 1320–1330.
31. Gao, Z.; He, X.; Chang, L. Accuracy Analysis of GPT3 Model in China. *Geomat. Inf. Sci. Wuhan Univ.* **2021**, *46*, 538–545.
32. Zhu, H.; Chen, K.; Huang, G. A Weighted Mean Temperature Model with Nonlinear Elevation Correction Using China as an Example. *Remote Sens.* **2021**, *13*, 3887. [[CrossRef](#)]
33. Long, F.; Gao, C.; Yan, Y.; Wang, J. Enhanced neural network model for worldwide estimation of weighted mean temperature. *Remote Sens.* **2021**, *13*, 2405. [[CrossRef](#)]

34. Durre, I.; Yin, X.; Vose, R.S.; Applequist, S.; Arnfield, J. Enhancing the data coverage in the integrated global radiosonde archive. *J. Atmos. Ocean. Technol.* **2018**, *35*, 1753–1770. [[CrossRef](#)]
35. Makama, E.K.; Lim, H.S. Variability and Trend in Integrated Water Vapour from ERA-Interim and IGRA2 Observations over Peninsular Malaysia. *Atmosphere* **2020**, *11*, 1012. [[CrossRef](#)]
36. Zhao, Q.; Yang, P.; Yao, W.; Yao, W. Adaptive AOD Forecast Model Based on GNSS-Derived PWV and Meteorological Parameters. *IEEE Trans. Geosci. Remote Sens.* **2021**, *60*, 5800610. [[CrossRef](#)]
37. Martin, A.; Weissmann, M.; Reitebuch, O.; Rennie, R.; Geiß, A.; Cress, A. Validation of Aeolus winds using radiosonde observations and numerical weather prediction model equivalents. *Atmos. Meas. Tech.* **2021**, *14*, 2167–2183. [[CrossRef](#)]
38. Zhao, Q.; Su, J.; Li, Z.; Yang, P.; Yao, Y. Adaptive aerosol optical depth forecasting model using GNSS observation. *IEEE Trans. Geosci. Remote Sens.* **2021**, *60*, 4105009. [[CrossRef](#)]
39. Van Zoest, V.M.; Stein, A.; Hoek, G. Outlier detection in urban air quality sensor networks. *Water Air Soil Pollut.* **2018**, *229*, 111. [[CrossRef](#)]
40. Bărbulescu, A.; Dumitriu, C.S.; Ilie, I.; Barbeş, S.-B. Influence of Anomalies on the Models for Nitrogen Oxides and Ozone Series. *Atmosphere* **2022**, *13*, 558.
41. Li, L.; Li, Y.; He, Q.; Wang, X. Weighted Mean Temperature Modelling Using Regional Radiosonde Observations for the Yangtze River Delta Region in China. *Remote Sens.* **2022**, *14*, 1909. [[CrossRef](#)]
42. Czernecki, B.; Głogowski, A.; Nowosad, J. Climate: An R package to access free in-situ meteorological and hydrological datasets for environmental assessment. *Sustainability* **2020**, *12*, 394. [[CrossRef](#)]
43. Sun, Z.; Zhang, B.; Yao, Y. An ERA5-based model for estimating tropospheric delay and weighted mean temperature over China with improved spatiotemporal resolutions. *Earth Space Sci.* **2019**, *6*, 1926–1941. [[CrossRef](#)]
44. Choi, B.I.; Lee, S.W.; Woo, S.B.; Kim, J.C.; Kim, Y.-G.; Yang, S.G. Evaluation of radiosonde humidity sensors at low temperature using ultralow-temperature humidity chamber. *Adv. Sci. Res.* **2018**, *15*, 207–212. [[CrossRef](#)]
45. Ding, J.; Chen, J. Assessment of empirical troposphere model GPT3 based on NGL’s global troposphere products. *Sensors* **2020**, *20*, 3631. [[CrossRef](#)]
46. Li, J.; Zhang, B.; Yao, Y.; Liu, L.; Sun, Z.; Yan, X. A refined regional model for estimating pressure, temperature and water vapor pressure for geodetic applications in China. *Remote Sens.* **2020**, *12*, 1713. [[CrossRef](#)]
47. Ding, M. A second generation of the neural network model for predicting weighted mean temperature. *GPS Solut.* **2020**, *24*, 61. [[CrossRef](#)]
48. Yu, H.; Miao, S.; Xie, G.; Guo, X.; Chen, Z.; Favre, A. Contrasting floristic diversity of the Hengduan Mountains, the Himalayas and the Qinghai-Tibet Plateau sensu stricto in China. *Front. Ecol. Evol.* **2020**, *8*, 136. [[CrossRef](#)]